Research Article

Optimum design and analysis of a dynamic energy management scheme for HESS in renewable power generation applications

Srinivas Punna[1] · Udaya Bhasker Manthati[1]

Abstract

A novel control strategy for a hybrid energy storage system (HESS) is outlined and examined in this paper. In the proposed system, the battery is utilized to stabilize the moderate changing of power surges, whereas supercapacitor is utilized to stabilize the rapidly changing of power surges. A two-loop proportional-integral controller is designed for the closed-loop operation of HESS. The source power and load power is not balanced because of the fluctuating conditions of photovoltaic (PV) power generation and load demand. This power imbalance causes fluctuations in direct current (DC) grid voltage. The DC bus voltage variations are mitigated using HESS, which is connected to DC grid through bi-directional DC–DC converter to enables the bidirectional power flow between energy storage devices and the DC bus. To enhance the life span and to reduce the current stress on the battery, the proposed method is employed with charge/discharge rate control feature. The proposed control procedure is realized in MATLAB/Simulink and the results are presented for different case studies. Experimental results are obtained for a two-input bi-directional converter at the sudden change in PV generation and load demand with the proposed controller. The proposed control strategy is effective for maintaining constant DC microgrid voltage under source and load fluctuations.

Keywords HESS · PI controller · SC · Battery · Photovoltaic (PV) · Bi-directional converter

1 Introduction

In the modern electrical grid system, interfacing of renewable energy sources (RES), electrical loads, and energy storage systems (ESS) made DC microgrid as an attractive technology. In light of natural resources utilize, low carbon emission and decentralized power system network resulted in more investigation in the area of distributed power generation (DG). The high energy density of energy storage systems is used to support the maximum power extraction from RES under all operating conditions [1]. Flywheel energy storage (FES), superconducting magnetic energy storage (SMES), supercapacitors (SC) and batteries are the few energy storage innovations used in RES power generation [2, 3]. However, there is no energy storage which can provide both fast dynamics as well as longer duration of the power.

The battery is the most used ESS in microgrid applications. However, they are suffering from high charging and discharging time (0.3–3 h) due to its low power density [4]. Battery reaction time is less under extraordinary load conditions, which results in reducing the life span of battery due to the high stress condition. There is another electrostatic storage device called supercapacitor or ultra-capacitor or electric double layer capacitor (EDLC). It is a high power density device and low energy density device with a fast dynamic response. So this is the driving inspiration for the hybridization of ESS with complementary characteristics. Which can provide both fast dynamic response and supply power for longer duration [5, 6]. This makes

✉ Srinivas Punna, srinu240@student.nitw.ac.in; Udaya Bhasker Manthati, ub@nitw.ac.in | [1]Department of Electrical Engineering, NIT-Warangal, Warangal, Telengana 506004, India.

the former an excellent choice for applications like hybrid electric vehicles (HEV) and microgrid applications.

In this way, a HESS was formed by combining high energy density battery and high power density supercapacitor [7–10]. In HESS, the ultimate objective is to control the power sharing between battery and supercapacitor. The charging/discharging of HESS is controlled through a two-input bidirectional converter and which interfaces HESS with DC microgrid. To exploit the advantages of both battery and SC, different topologies of HESS were introduced for DC microgrid applications. Interfacing of multiple energy storage systems as a buffer to isolate the load fluctuations from the shipboard network was presented in [11]. A multiple input (MI) isolated buck-boost converter is presented in [12]. Between the sources they have galvanic isolation and magnetic coupling for power sharing among battery and SC sources in these converters. Various sources aided with multiple bidirectional boost converters are used to supply required DC power and changed over into AC power [13, 14]. Distinctive control techniques have been represented for convincing voltage regulation of DC microgrid [15–20].

The paper is organized as follows: Sect. 2 introduces the literature review and background of the research work is quickly portrayed. Section 3 depicts the configuration of HESS supported renewable energy generation system. In Sect. 4 the proposed novel HESS control strategy is depicted. Design of the proposed controller for HESS is described in Sect. 5. Simulation results are presented in Sect. 6. Experimental results are presented in Sect. 7. Results and inferences are concluded in Sect. 8.

2 Recent research works: a brief review

Different research works have beforehand existed in the literature which relied upon the interfacing of HESS to a DC microgrid. The motivation behind the control techniques is to maintain the DC bus voltage constant. A section of the works is assessed here.

Kollimalla et al. [21] have illustrated a control scheme for power sharing between SCs and batteries. The introduced control strategy regulate the DC link voltage for any mismatch between PV generation and load demand. The battery supplies the average power requirement while the SC supplies the fast transient power demand in addition to battery error current. This additional feature not just enhances the capability of voltage regulation in the DC grid also reduces the stress level on the battery and henceforth enhance the battery life span. However, the designed system is not validated with state of charge (SOC) variations of ESS. For battery energy storage, a two stage control with variable rate-limit was presented in the work [22].

The main objective of the control scheme is to improve the amount, rate, and duration of time of charging/discharging of the battery. SC is used to supply power during the transient period. By optimizing the battery current rates, the stress levels of battery were controlled. For PV aided DC grid system, with HESS was illustrated by Manandhar et al. [23]. To expand the overall performance of HESS, this methodology uses the battery uncompensated power.

Amid the peak PV generation and voltage drop, while meeting the peak load, battery energy storage (BESS) systems were utilized to eliminate voltage rise problem was presented by Zeraati et al. [24]. A distributed control scheme is designed to overcome the limits of a coordinated control strategy. To keep the excessive saturation or batteries depletion changes under control, the performance of BESs are designed considering their State of Charge (SOC). As far as their installed capacity the main algorithm decides the BESs participation in voltage regulation.

In PV generation, the system configuration of ramp-rate control with energy storage devices was presented by Perdana et al. [25]. To reduce the number of power converters and improve system efficiency, the direct connection of HESS was executed. Both battery bank and ultra-capacitor unit called a HESS scheme was clarified by Akta et al. [26]. By an energy management algorithm, depending upon the dynamic changes in the system was executed. Yi et al. [27] developed unified control of energy management system for PV-battery based grid connected and islanded operation has been presented. In the proposed control strategy, battery balances the AC microgrid and DC microgrid in all different operating conditions. This increases the stress on the battery, system cost and reduces life cycle of the battery.

2.1 Background of the research work

The review of the recent research work exhibits that the HESS interfacing to a DC microgrid with the motivation behind voltage control as a critical contributing element. In the microgrid the variable nature of renewable power sources can't meet the load demand alone. To ensure the continuous power supply to the load, ESS is integrated with RES power generation. In any case, there are various techniques have been executed for the regulation of the DC grid voltage with the aid of ESS, for instance, two-stage variable rate-limit control, battery bank and the ultra-capacitor unit, self-organizing map, particle swarm optimization etc.

The fundamental thought behind all the control schemes is that supercapacitor is managed the high-frequency power component and the battery is to manage average power component. Regardless, most of the

different plans didn't consider voltage regulation of the DC grid in the fluctuation of power. At the point when worked under high power changes the batteries are slanting to failure of premature. In this way, to upgrade the life span and stress level on the battery is the basic issue found in the literary works. Likewise, from the previously mentioned written works clearly for DC microgrid application, multiple-input bidirectional converters required for power flow control between load and ESS. To overcome the previously mentioned difficulties, an optimal control strategy for HESS interfaced with the multiple-input bidirectional converter is required.

3 HESS supported RES configuration

The most commonly used configuration of HESS, which has the leverage of attaining independent control on both battery and SC is as shown in Fig. 1. In this active parallel configuration of HESS, it is possible to exchange energy between the component ESSs, for example, the battery ESS can charge supercapacitor ESS or vice versa. For the DC microgrid, PV is the main source of power and connected with battery and supercapacitor. The boost converter is used for maximum power point (MPP) extraction
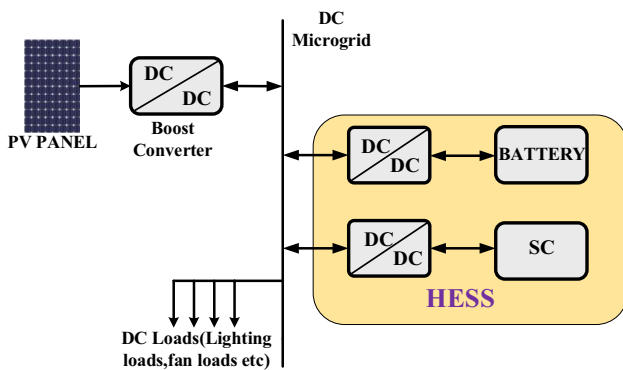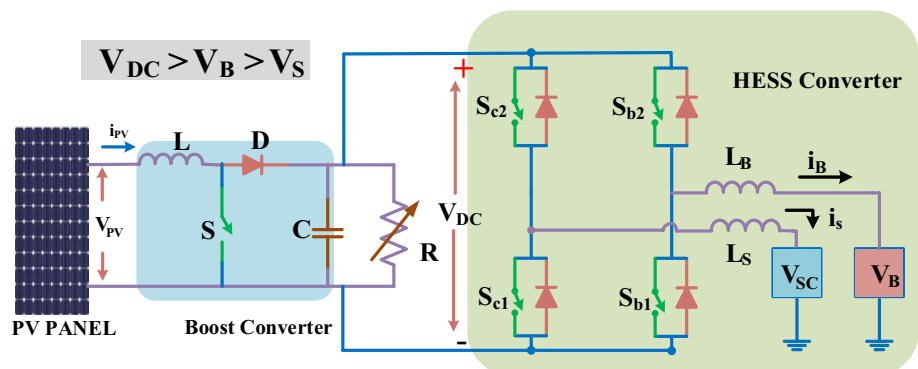
and interfacing of PV to DC microgrid. In the present work PV source is rated at MPP voltage 12.2 V, MPP current: 1.4 A and maximum power: 16.8 W at a solar irradiance 1000 W/m^2 and cell temperature 25 °C. By utilizing the HESS system including battery-SC bank, mismatch among source power and load power is settled. A two-input 4 switch H-bridge bidirectional converter is used to connect HESS with DC microgrid. With the usage of the 2-input bidirectional converter, HESS charging and discharging is controlled. At the point of mismatch between source power and load power, HESS take care of the surplus or deficient power at the set reference of grid voltage.

3.1 Operation of microgrid with HESS

The operation of microgrid with HESS is cleared up in this subsection and two-input bidirectional converter is used to HESS (charging/discharging) control. The system involves 4 bidirectional switches which are organized in the topology of H-bridge showed up in Fig. 2. Battery voltage is selected to be less than that of DC grid voltage but greater than SC voltage in this converter topology. High frequency inductors L_B and L_S are connected to the battery and SC legs respectively. Different modes of operation are explained in the following sections.

3.1.1 HESS charging mode

Whenever generated PV power exceeds the load requirement or load demand decreases, so excess power existing in the DC microgrid which results DC grid voltage increases. This excess amount of power will charge both battery and supercapacitor to stabilize DC microgrid. Hence in this mode power flows from DC microgrid to HESS. The converter operation in this mode can be divided into two time intervals as shown in Fig. 3. During the time interval T_1, switches S_{b2} and S_{c2} as switches are operated with duty cycle, charging both the inductors L_B and L_S by corresponding sources V_B and V_{SC}. Current increases with a slope of $(V_{DC} - V_B)/L_B$ and $(V_{DC} - V_{SC})/L_S$ respectively as

Fig. 1 PV based microgrid aided by HESS

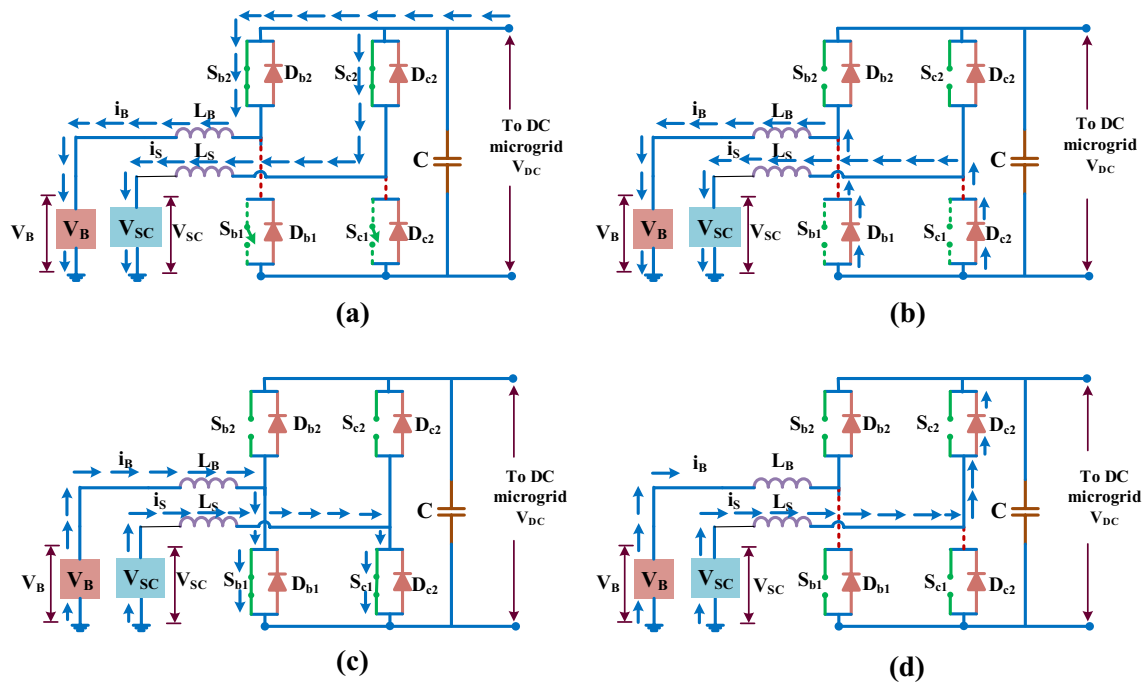**Fig. 2** DC microgrid setup powered by PV source and supplemented by HESS

Fig. 3 Equivalent circuit of bidirectional DC–DC converter for charging and discharging mode

demonstrated in Fig. 3. At the end of this interval (during T_2), both the switches are turned off providing freewheeling path for i_{LB} and i_{LS} through D_{b1} and D_{c1} respectively.

$$V_B = d_B \cdot V_{DC} \tag{1}$$

$$V_{SC} = d_{SC} \cdot V_{DC} \tag{2}$$

where d_B and d_{SC} are the duty cycles. Transfer of energy from DC grid to HESS. The DC grid has extreme potential than the HESS. In order to HESS charge, then the converter is operated as buck mode.

3.1.2 Discharging mode of HESS

DC microgrid voltage decreases if load exceeds PV generation capability or when PV generated power falls due to reduced solar irradiation. During this time interval power has to be supplied by HESS. By operating on devices S_{b1} and S_{c1}, power flows from HESS to DC microgrid in this mode, by properly controlling bidirectional converter. During the time interval T_3, switches S_{b1} and S_{c1} are gated-on, inductors (L_B and L_S) stores energy in opposite direction, reverse currents (i_{LB} and i_{LS}) increases with a slope of V_B/L_B and V_{SC}/L_S respectively as demonstrated in Fig. 3. After end of this time period T_3 (during time period T_4) as sum of battery and inductor voltages exceeds DC microgrid voltage, so power flows from HESS to DC microgrid current directions of each time interval as demonstrated in Fig. 4.
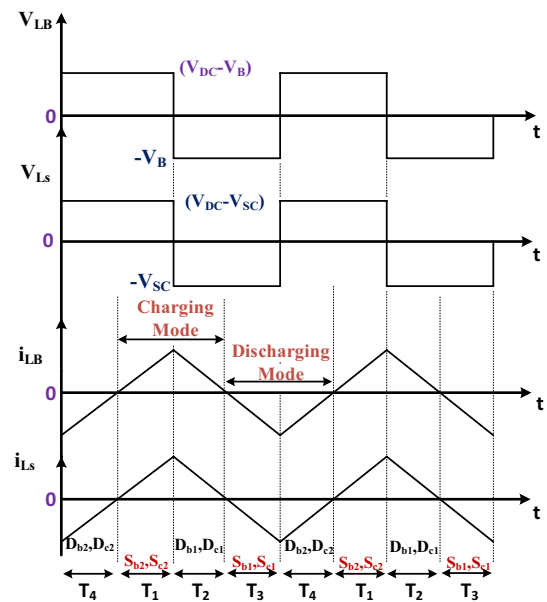

Fig. 4 Steady state waveforms for HESS charging discharging mode

$$V_{DC} = \frac{V_B}{1 - d_B} \tag{3}$$

$$V_{DC} = \frac{V_{SC}}{1 - d_{SC}} \tag{4}$$

Since S_{b1}, S_{b2}, S_{c1}, and S_{c2} are the switches which are switched in the complimentary way. For each switching leg, only 1 gate circuit is required.

4 Proposed control strategy of HESS

The control block diagram of conventional and proposed control schemes are depicted in Fig. 5. To the proportional integral (PI) controller, the reference ($V_{DC,ref}$) and actual (V_{DC}) voltages of grid are contrasted with each other in both schemes and the dissimilarity in voltages is proceed. From the HESS the controller is generating total reference current (i_{tot}) required and which is minimizing the difference in voltages. In the conventional scheme total current is decomposed into frequency components as low and high range, to the battery and SC which is given as reference currents respectively and it is depicted in Fig. 5a. The reference current of SC consists of a component with high frequency and the battery current with error component in the proposed control scheme which is explained below,

The component (i_{lfc}) with low frequency is derived from i_{tot} as derived as follows,

$$i_{lfc} = f_{lfc}(i_{tot}) \tag{5}$$

where low pass filter function is represented as $f_{lfc}(.)$. A rate limiter (f_{rl}) is introduced for battery current charge/discharge rate limit which is depicted in Fig. 5b. The current signal reference of rate limiter output is formulated by,

$$i_{BAT,ref} = f_{rl}(i_{lfc}) \tag{6}$$

The difference in currents ($i_{BAT,err}$) is given to the PI controller after the battery current with reference and actual are contrasted with each other. The controller generates the control signal (d_B) to minimize the dissimilarity in the currents. The pulse width modulated (PWM) pulses are generated to the switches (S_{b1}, S_{b2}) in the converter of battery to the PWM generator, this duty ratio which is shown in Fig. 5b. In DC–DC converter due to the electrical inertia and slow dynamics of battery system the converter may not follow instantly with battery reference current ($i_{BAT,ref}$). Therefore, the uncompensated power is observed in battery system is given by

$$i_{tran} = i_{tot} - i_{BAT,ref} \tag{7}$$

$$P_{B\_Uncomp} = (i_{BAT,ref} - i_{BAT}) \cdot V_B \tag{8}$$

Fig. 5 **a** Control block diagram of conventional control schemes, **b** control block diagram of proposed control schemes
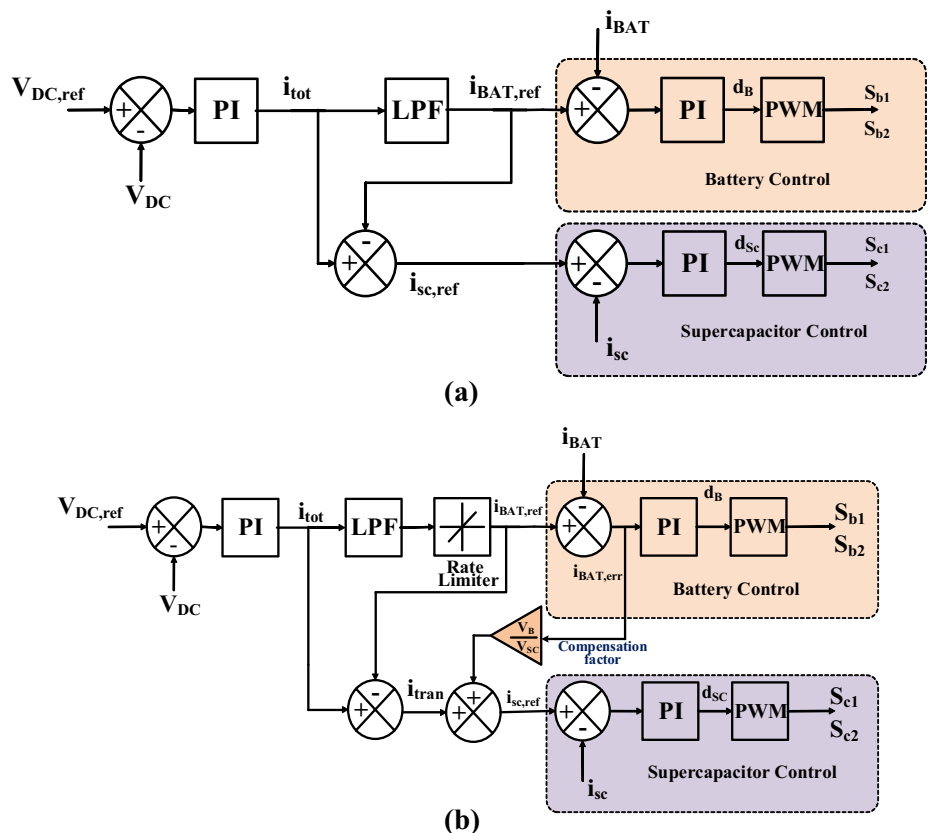
where i_{tran} transient component of current, P_{B_Uncomp}: battery uncompensated power. In the proposed control strategy P_{B_Uncomp} used to enhance the performance of SC. Therefore, the supercapacitor reference current ($i_{SC,ref}$) is formulated as follows,

$$i_{SC,ref} = i_{tran} + \left(i_{BAT,ref} - i_{BAT}\right)\frac{V_B}{V_{SC}} \qquad (9)$$

The error is passed to the controller after the actual and references of supercapacitor currents are contrasted with each other. The error is minimized when the PI controller generates the control signal d_{SC}. To generate the pulses of PWM corresponding to SC switches such as S_{c1}, S_{c2} this control signal is given to the PWM generator which is shown in Fig. 5.

$$i_{SC,ref} = i_{tran} + i_{BAT,err} \cdot \frac{V_B}{V_{SC}} \qquad (10)$$

where $i_{BAT,err}$: battery error current is the difference between actual and references of battery is given by

$$i_{BAT,err} = i_{BAT,ref} - i_{BAT}$$

5 Design of proposed controller for HESS

The design of proposed controller for HESS is clarified [28]. In the unified controller a single controller is utilized to trigger the two control switches. For both charge (buck) and discharge (boost) modes [29, 30], boost mode of operation is considered to design the controller. The sub-harmonic oscillations are kept then, the current control loop bandwidth of supercapacitor controller is restricted to 0.1667 times switching frequency and it is spoken to as (f_{sw}) [31]. Here, the switching frequency is equivalent to 10 kHz. The battery current controller Bandwidth (BW) is

chosen with the end goal that high frequency transients are redirected to supercapacitor, i.e. at $f_{sw}/10$. In stable region to work the system, the bandwidth of the converter must be worked significantly lesser than the right half plane zero frequency (f_{rhpz}) [32] of the supercapacitor.

$$f_{RHPZ} = \frac{(1 - d_{SC})^2 R}{2\pi L_S} \qquad (11)$$

where R: load resistance, L_S: SC inductance and d_{SC}: duty cycle of SC leg. The outer voltage control loop is slower than the inner current control loop; than the voltage control loop bandwidth is picked lesser than that of the SC current control loop.

5.1 Design of supercapacitor current controller

Figure 6 shows the block diagram of the current controller of the supercapacitor. The voltage control loop produces the supercapacitor reference current ($i_{sc,ref}$) in the controller. In the current control loop, reference current is contrasted with the actual current [33]. After perturbation and linearization of state equations, duty cycle to SC current transfer function is given below,

$$G_{id\_SC} = \frac{\hat{i}_{SC}}{\hat{d}_{SC}} = \frac{V_{DC}CS + 2\frac{V_{DC}}{R}}{L_S CS^2 + \frac{L_S}{R}S + (1 - d_{SC})^2} \qquad (12)$$

Here, the duty cycle of small perturbations as $\hat{d}_{SC}$, SC inductor current as $\hat{i}_{SC}$. The PI control transfer function of SC current loop is formulated as follows,

$$G_{pi,SC} = K_{p,SC} + \frac{K_{i,SC}}{S} \qquad (13)$$

Here, proportional and integral gains of the PI controller is represented as $K_{p,SC}$ and $K_{i,SC}$.

Controller parameters ($K_{p,SC}$ and $K_{i,SC}$) for inner current loop is designed based on above model with bandwidth
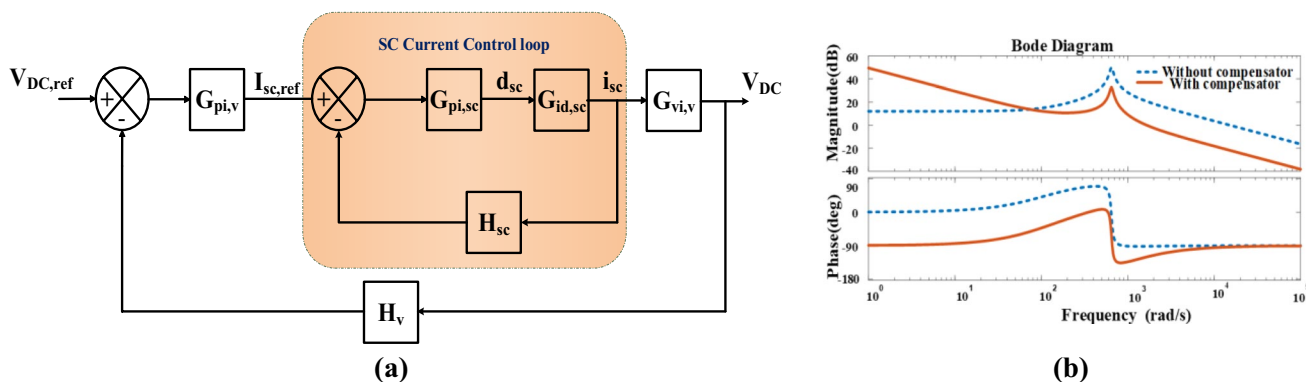

Fig. 6 **a** SC controller Block diagram. **b** Bode plot of inner current controller of SC control logic with controller

of 1.67 kHz and phase margin of 59.2°. Bode plot for compensated and uncompensated transfer functions is shown in Fig. 6b. The controller parameters are designed and fine-tunes using SISO tool in MATLAB software. The proportional and integral constants obtained are 0.0088 and 80.689 respectively.

The open loop transfer function of SC current controller can be calculated based on the following equation,

$$G_{ol,SC} = G_{pi,SC} \cdot G_{id,SC} \cdot H_{SC} \qquad (14)$$

Here, gain of the current sensor is specified as H_{SC}.

5.2 Design of HESS voltage controller

The voltage control loop, SC current to voltage small signal transfer function are obtained in Eq. (15).

$$G_{vi,v} = \frac{\overset{\wedge}{V_{DC}}}{\overset{\wedge}{i_{SC}}} = \frac{R(1 - d_{sc}) \cdot \left(1 - \frac{L_{sc}}{R(1-d_{sc})^2}S\right)}{2 + RCS} \qquad (15)$$

Here, the output voltage small perturbation is specified as $\overset{\wedge}{V_{DC}}$. The PI control transfer function of voltage control loop is given as follows,

$$G_{pi,v} = K_{p,v} + \frac{K_{i,v}}{S} \qquad (16)$$

Here, the PI controller gains as $K_{p,v}$ and $K_{i,v}$. Open loop transfer function of voltage controller is equated as follows,

$$G_{ol,v} = G_{pi,v} \cdot G_{cl,sc} \cdot G_{vi,v} \cdot H_v \qquad (17)$$

Here, $\quad G_{cl,sc} = \dfrac{G_{pi,sc} \cdot G_{id,sc}}{1 + G_{pi,sc} \cdot G_{id,sc} \cdot H_{sc}} \qquad (18)$

Here, gain of the voltage sensor is represented as H_v.

Proportional constants of outer voltage loop is also designed based on averaged state space model. Bandwidth has to be less than right half plane zero. The designed voltage controller has a bandwidth of 200 Hz and phase margin 59.2°. Bode plot for compensated and uncompensated transfer functions shown in Fig. 7. Proportional and integral constants are 5.96 and 175 respectively.

5.3 Battery current controller design

Figure 8a depicts the block diagram of the battery current controller. The duty cycle to battery current transfer function for battery stage is given by,
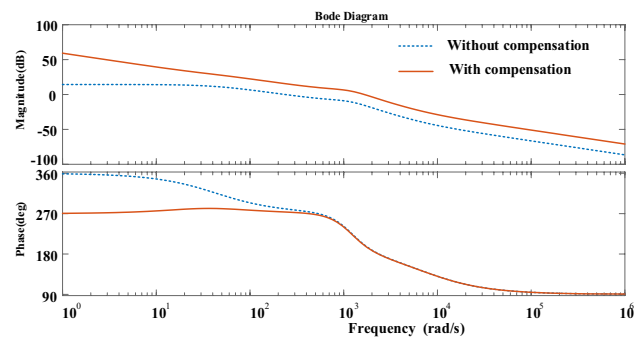
Fig. 7 Bode plot of outer voltage controller of supercapacitor control logic with controller

$$G_{id,BAT} = \frac{\hat{i}_{BAT}}{\hat{d}_B} = \frac{V_{DC}CS + 2\frac{V_{DC}}{R}}{L_BCS^2 + \frac{L_B}{R}S + (1 - d_B)^2} \qquad (19)$$

Here, small perturbations in duty cycle as $\hat{d}_B$, battery inductor current is represented as $\hat{i}_{BAT}$.

The PI control transfer function of battery current control loop as follows,

$$G_{pi,BAT} = K_{p,BAT} + \frac{K_{i,BAT}}{S} \qquad (20)$$

Here, proportional and integral gains of the PI compensator as $K_{p,BAT}$ and $K_{i,BAT}$. The open loop transfer function of current control loop is formulated as follows,

$$G_{ol,BAT} = G_{pi,BAT} \cdot G_{id,BAT} \cdot H_{BAT} \qquad (21)$$

Here, gain of the current sensor is represented as H_{BAT}.

PI controller to regulate battery current is designed based on above transfer function. Bandwidth of the controller is made less than that of supercapacitor controller stage. The designed controller has a bandwidth of 1 kHz with phase margin of 59.2°. Bode plot of compensated and uncompensated plant is shown in Fig. 8b. The proportional and integral constants obtained are 0.1404 and 78 respectively.

6 Simulation results and discussion

In simulation, PV panel is emulated as current regulated voltage source using boost converter for step change in source power. The control procedure is made using Simulink blocks in MATLAB. The system parameters used for simulation and experimental results are presented in Table 1. For boost and bi-directional DC–DC converters, MOSFET switches are chosen. The ultimate aim of the proposed system is to stabilize the DC-link voltage for any
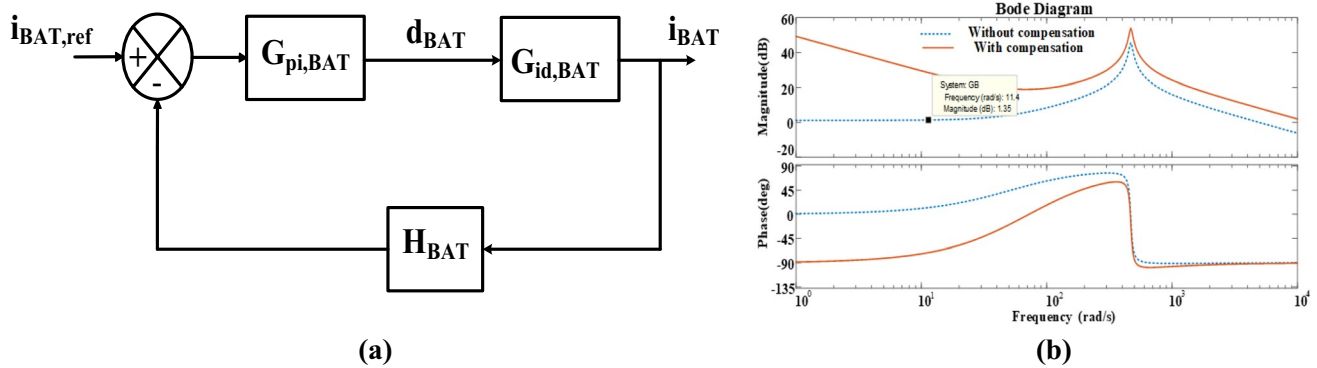
Fig. 8 **a** Battery current controller block diagram. **b** Bode plot of battery current controller

Table 1 System parameters for simulation and experimental study

S. no	Parameter	Value
1	MPPT voltage (V_{pv})	12 V
2	MPPT current (i_{pv})	1.4 A
3	SC voltage (V_S)	10 V
4	SC inductance (L_S)	1.43 mH
5	Battery voltage(V_B)	12 V
6	Battery inductance (L_B)	4.8 mH
7	Boost inductance (L_s)	4.1 mH
8	Resistance (R)	25 Ω
9	DC grid voltage (V_{DC})	20 V
10	Capacitance (C)	150 µF

disturbance occur in load side as well as source side. In this segment, the results of the proposed technique analysis is developed by two test cases are considered.

Case 1 Stabilization of DC grid against step variation in PV Generation
Case 2 Stabilization of DC grid against step variation in load

Case 1 Stabilization of DC grid against step variation in PV generation

6.1 Step increase in PV generation

Figure 9 demonstrates the step variation of PV generation over the period of time frame. Due to the atmosphere variations power produced by the PV panel increases to 40 W from 30 W at t = 0.2 s by this is emulated by increasing PV current to 2 A from 1.5 A. As input power is more than load power can consume, grid voltage increases more than 20 V. Than immediately SC absorbs the excess power of 10 W in short duration of time until battery can regulate the grid voltage to 20 V. Thus battery and supercapacitor

charge accordingly to maintain the DC grid voltage constant at 20 V. Figure 9 shows the battery current waveform with reduced current stress due to low current charge rate. At the point when a bi-directional converter is associated among battery and supercapacitor, the DC grid voltage is recovered back to steady state in approximately in 10 ms.

6.2 Step decrease in PV generation

Due to the atmosphere variations power produced by the PV panel decreases to 30 W from 40 W at t = 0.4 s by this is decreasing PV current to 1.5 A from 2 A. As input power is less than load power can results, DC grid voltage is less than 20 V. Than immediately discharge SC for deficient power of 10 W in short term until battery can regulate DC grid voltage to 20 V. By this manner a bi-directional converter is associated among battery and supercapacitor, the DC grid voltage is recovered back to 20 V utilizing the proposed control strategy.

Case 2 Stabilization of DC grid against step variation in load

The output power produced by the PV panel is 16 W in maximum power region. A load resistance of 25 Ω is connected to 20 V DC microgrid. In steady state load draws 0.8 A current thereby consuming the entire power generated by PV panel. For step variation in load, load resistance decreased to 18 Ω at t = 0.2 s for duration of 0.4 s. Then load requirement increases to 27 W from 16 W which is more than power range of PV panel. Due to source and load power imbalance DC grid voltage falls below 20 V. Now control logic will sense any deviation from DC grid voltage reference of 20 V and controls the bi-direction converter associated with battery and supercapacitor will now supply excess power of 11 W in 10 ms duration of time with increased load. In this mode both battery and supercapacitors are discharging. Figure 10 shows the battery and supercapacitor current waveforms, stress on battery current reduced with help of SC.
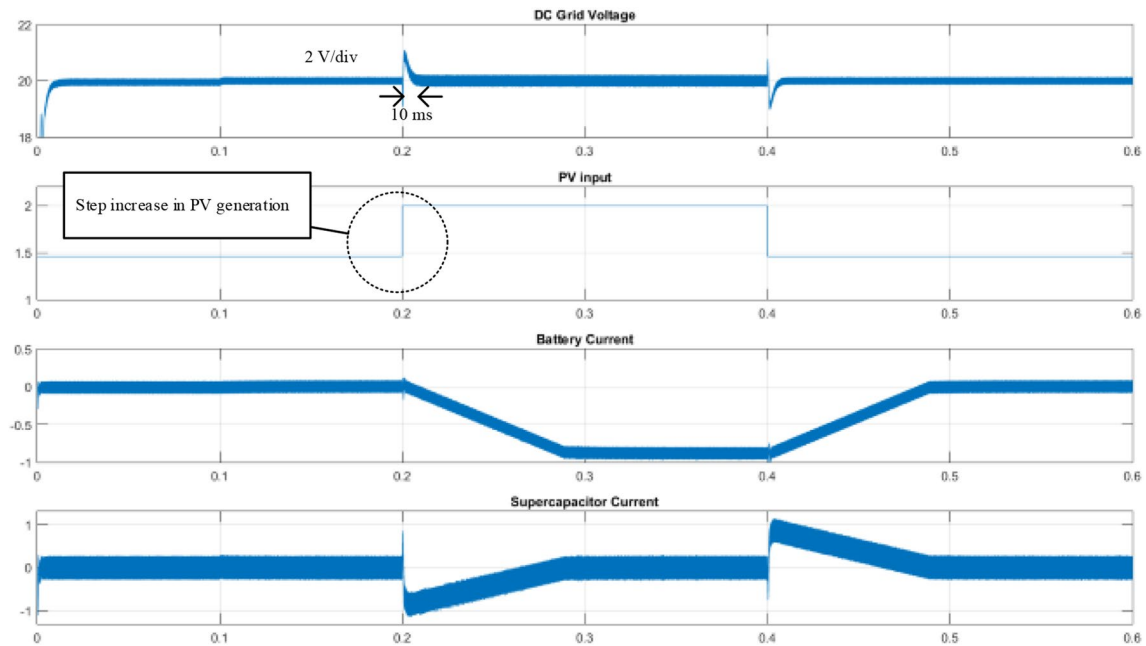
Fig. 9 Grid voltage, PV input current, battery current and SC current waveforms for step variation in PV generation
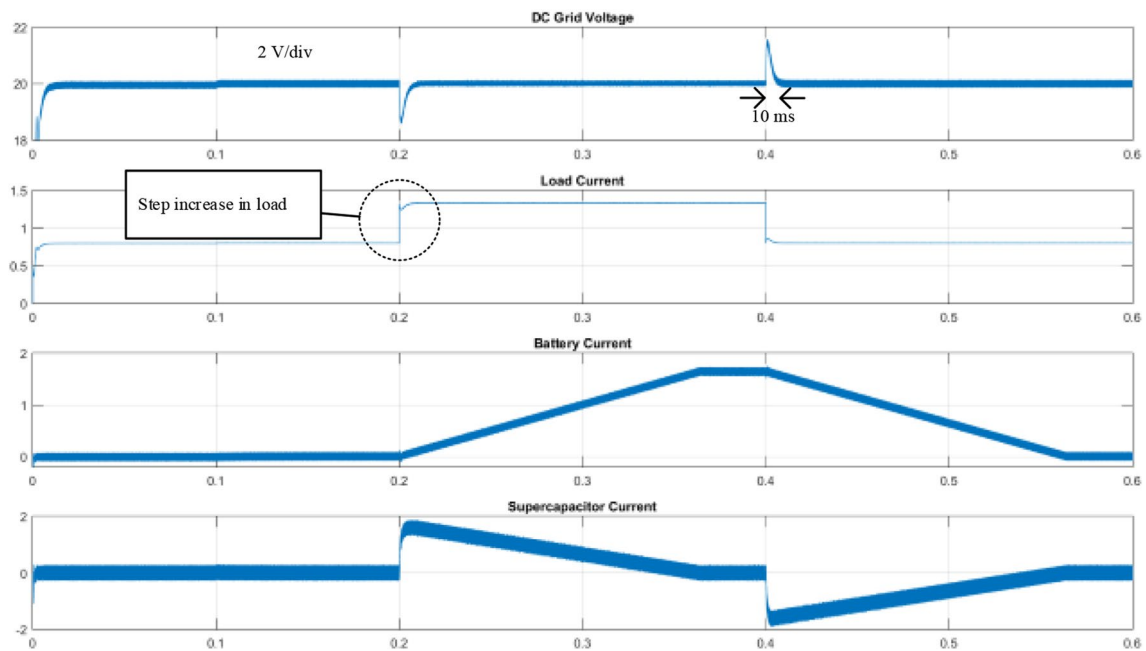

Fig. 10 DC grid voltage, load current, battery current and SC current waveforms for step load variation

7 Experimental results

A low power hardware prototype is developed for proposed controller for two-input bidirectional converter shown in Fig. 11. The controller used for this experiment is dSPACE DS1104. In this experiment a regulated power supply (RPS) is used as PV generator. RPS currents are controlled by using boost converter. Exide chloride 12 V, 7 Ah lead acid battery and Maxwell BMOD0058 16 V, 58 F supercapacitor. The two input bidirectional converter is built using four MOSFET switches IRF540N. Operation of microgrid with HESS in charging and discharging mode explained in Sect. 3. DC grid specifications are given in

Fig. 11 Prototype model of the proposed topology

Fig. 12 **a** Experimental results for HESS charging mode: DC microgrid voltage (V_{DC}), battery current (i_B), supercapacitor current (i_S). **b** Supercapacitor SOC waveform
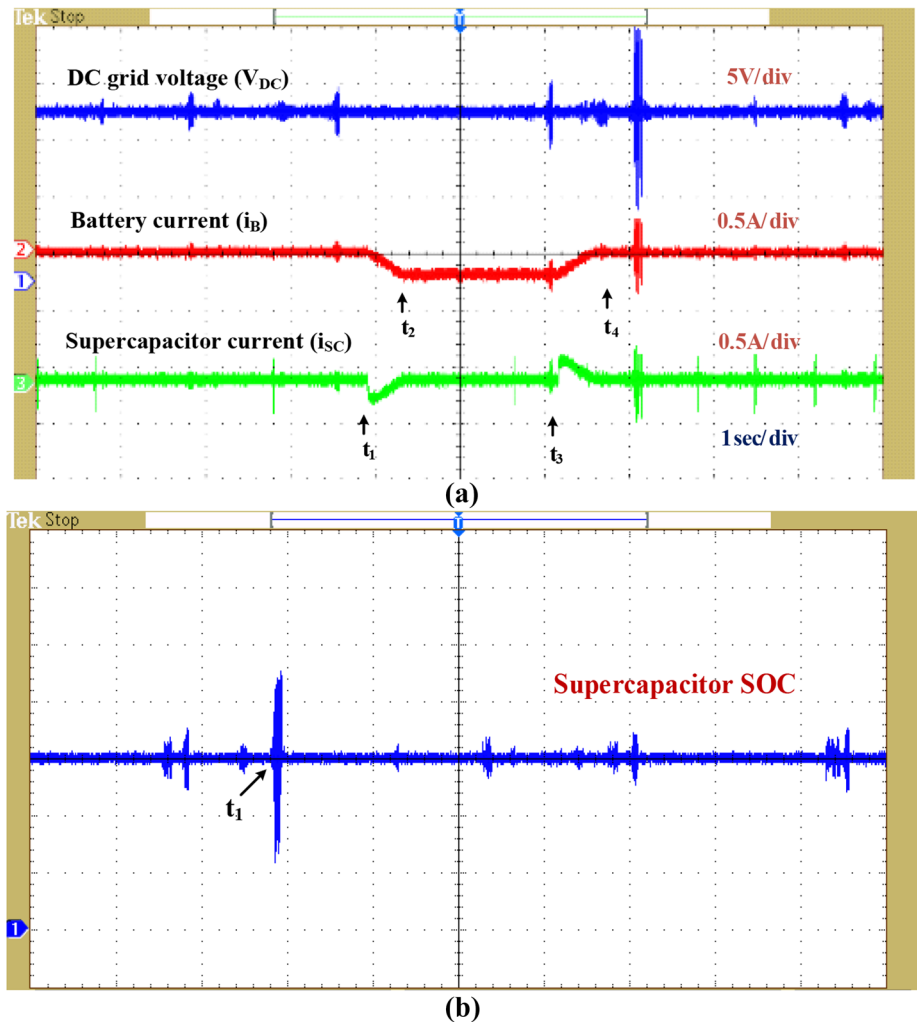

(a)

(b)

Fig. 13 Experimental results for HESS discharging mode: DC microgrid voltage (V_{DC}), battery current (i_B), supercapacitor current (i_s) and state of charge of supercapacitor. **b** Supercapacitor SOC waveform
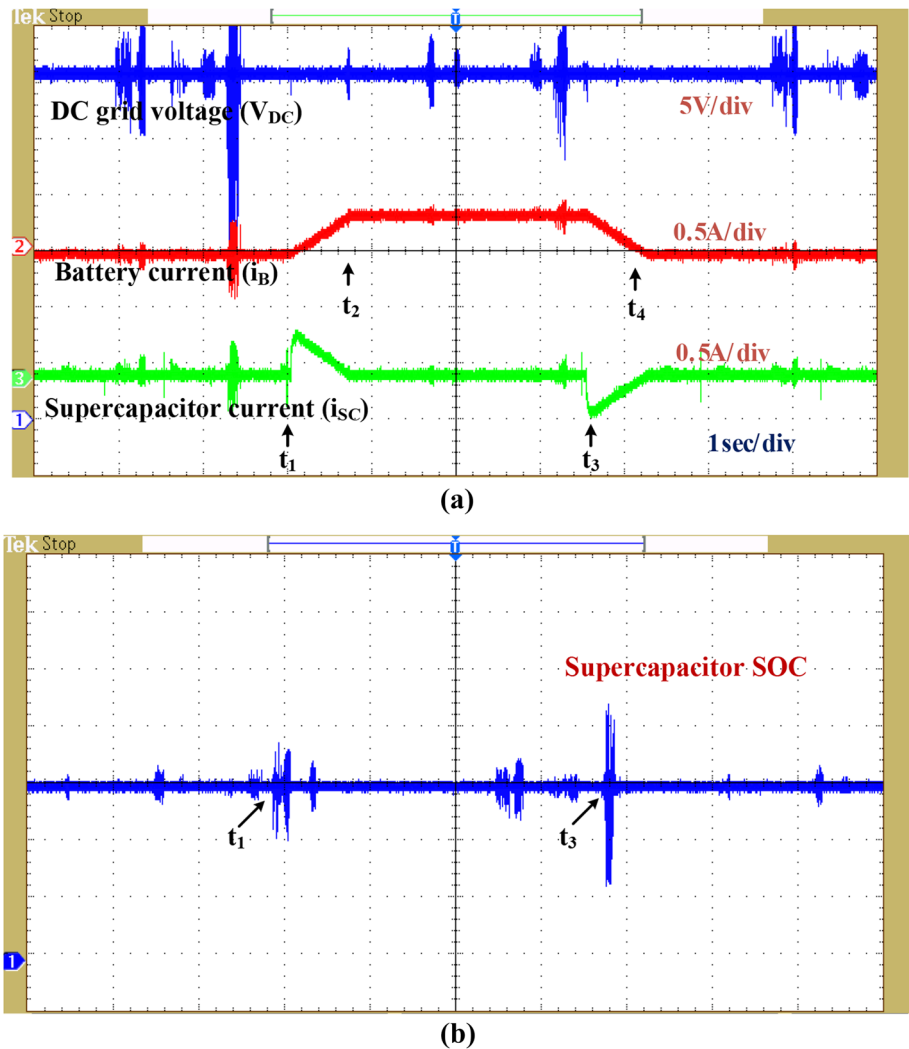

(a)

(b)

Table 1. DC microgrid is setup at a nominal voltage of 20 V.

7.1 HESS charging mode

Here controller designed for scenario of surge in DC grid voltage by increasing PV generation (or) decrease in load is analyzed. The waveforms are shown in Fig. 12.

A sudden upward movement in microgrid voltage is realized by increasing PV generation. Initially $I_{PV} = 1.3$ A and at time $t = t_1$, I_{PV} is increased to 1.42 A and as a result increased in PV generation. The excess energy in DC grid cause a surge in grid voltage. Immediately HESS responds, Transient component of current charging supercapacitor and battery charging current is allowed to increase slowly till steady state value at instant $t = t_2$. The PV generation brought back to original condition of $I_{PV} = 1.3$ A at instant $t = t_3$. Battery and supercapacitor then return to its floating state as it was before $t = t_1$. At instant t_1 and t_3 DC microgrid voltage is retained at 20 V almost instantly as indicated by

small spikes in the Fig. 12a. Supercapacitor SOC shown in Fig. 12b. At the instant t_1, SOC_{SC} is shown to be increasing indicating charging of supercapacitor. After transient current has died out, supercapacitor remains idle as indicated by constant SOC. Battery SOC is not considered, its energy not depleted fast compared to supercapacitor.

7.2 HESS discharging mode

Discharging mode is active either due to decrease in PV generation or due to increase in load. Waveforms are shown in Fig. 13.

Here, dip in microgrid voltage is realized by an increase in load. At instant t_1, R is decreased from 25 to 18 Ω. This causes DC microgrid voltage to dip since there exists a power mismatch between source and load. The deficient power is then fed by HESS by discharging battery and supercapacitor. Transient current is met by supercapacitor and steady state current is supplied by battery as is evident from current waveforms. Combined action of

battery and supercapacitor maintain DC microgrid voltage constant at nominal value of 20 V. Small spike in voltage waveform in Fig. 13a is negligible due to fast dynamic of HESS. At instant t_3, R is reverted back to normal setting of 25 Ω and V_{DC} is brought to 20 V again. Supercapacitor SOC waveform is also shown in Fig. 13b to validate the above explained operation. When load demand increased at instant t_1, SOC_{SC} is found to be decreased as long as supercapacitor supplies current indicating discharge operation of supercapacitor. After that supercapacitor is idle as indicated by constant SOC waveform. Similarly at instant t_3, SOC increased to indicate charging of supercapacitor after which it stays idle.

8 Conclusion

In this paper, a controller is designed for two input bi-directional converter with battery and supercapacitor as storage system. Performance of the HESS is analyzed for the source and load variation case using proposed control strategy. Controller could effectively stabilize DC microgrid against the source and load variation. Charging and discharging waveforms of the battery are observed during source and load variation. The operation of energy balance forces severe stress on battery, if battery alone as an energy storage medium. This is principally resulted in battery with low power density. Along these lines, supercapacitor with high power density is joined with high energy density battery utilizing proposed control technique to share the imbalance power exist between microgrid of source and load. This unified controller provided to be enough for both charging and discharging operation of HESS. Moreover, decoupled, separate and independent control of supercapacitor and battery power was achieved as well as power flow between them. It can also be used in the case of hybrid electric vehicle applications where more than two power supply. The proposed method includes less CPU time. Hence it makes HESS with high power and energy density, which extended the life of battery.

Compliance with ethical standards

Conflict of interest The authors declare that they have no conflict of interest.

References

1. Gee A, Robinson F, Dunn R (2013) Analysis of battery lifetime extension in a small-scale wind-energy system using supercapacitors. IEEE Trans Energy Convers 28(1):24–33
2. Karki R, Billinton R (2001) Reliability/cost implications of PV and wind energy utilization in small isolated power systems. IEEE Trans Energy Convers 16(4):368–373
3. Shimizukawa J, Iba K, Hida Y, Yokoyama R (2010) Mitigation of intermittency of wind power generation using battery energy storage system. In: Proc. 45th int. conf. univ. power eng., pp 1–4
4. Glavin M, Chan P, Armstrong S, Hurley W (2008) A stand-alone photovoltaic supercapacitor battery hybrid energy storage system. In: IEEE power electronics and motion control conference, pp 1688–1695
5. Shen J, Khaligh A (2015) A supervisory energy management control strategy for a battery/ultra capacitor hybrid energy storage system. IEEE Trans Transp Electrific 1(3):223–231
6. Li J et al (2015) Design and advanced control strategies of a hybrid energy storage system for the grid integration of wind power generations. IET Renew Power Gener 9(2):89–98
7. Serban I, Marinescu C (2014) Battery energy storage system for frequency support in Microgrids and with enhanced control features for uninterruptible supply of local loads. Int J Electr Power Energy Syst 54:432–441
8. Jia Y, Shibata R, Yamamura N, Ishida M (2006) Characteristics of smoothed-power output topology of stand-alone renewable power system using EDLC. In: Proc. 37th IEEE conf. power electron. spec., pp 1–7
9. Ding M, Wang B, Chen Z, Chen Z, Luo Y, Zheng G (2012) Stabilizing control strategy of complementary energy storage in renewable energy system. In: Proc. Asia IEEE innovative smart grid technol., pp 1–5
10. Dubal DP, Ayyad O, Ruiz V, Gomez-Romero P (2015) Hybrid energy storage: the merging of battery and supercapacitor chemistries. Chem Soc Rev 44:1777–1790
11. Hou J, Sun J, Hofmann H (2018) Control development and performance evaluation for battery/flywheel hybrid energy storage solutions to mitigate load fluctuations in all-electric ship propulsion systems. Appl Energy 212:919–930
12. Choi ME, Kim S-W, Seo S-W (2012) Energy management optimization in a battery/supercapacitor hybrid energy storage system. IEEE Trans Smart Grid 3(1):463–472
13. Moseley P (2006) Energy storage in remote area power supply (RAPS) systems. J Power Sources 155(1):83–87
14. Mendis N, Muttaqi K, Perera S (2014) Management of battery-supercapacitor hybrid energy storage and synchronous condenser for isolated operation of PMSG based variable-speed wind turbine generating systems. IEEE Trans Smart Grid 5(2):944–953
15. Laldin O, Moshirvaziri M, Trescases O (2013) Predictive algorithm for optimizing power flow in hybrid ultracapacitor/battery storage systems for light electric vehicles. IEEE Trans Power Electron 28(8):3882–3895
16. Kim MY, Kim JH, Moon GW (2014) Center-cell concentration structure of a cell-to-cell balancing circuit with a reduced number of switches. IEEE Trans Power Electron 29(10):5285–5297
17. Hsieh YH, Liang TJ, Chen SMO, Horng WY, Chung YY (2013) A novel high-efficiency compact-size low-cost balancing method for series connected battery applications. IEEE Trans Power Electron 28(12):5927–5939
18. Lee WC, Drury D, Mellor P (2011) Comparison of passive cell balancing and active cell balancing for automotive batteries. In: Proc. IEEE conf. vehicle power propulsion, pp 1–7
19. Chen S, Chen CC, Huang HP, Hwu CC (2011) Implementation of cell balancing with super-capacitor for robot power system. In: Proc. 9th world congr. intell. control autom., pp 468–473
20. Lahyani A, Venet P, Guermazi A, Troudi A (2013) Battery/supercapacitors combination in uninterruptible power supply (UPS). IEEE Trans Power Electron 28(4):1509–1522

21. Kollimalla S, Mishra M, Narasamma NL (2014) Design and analysis of novel control strategy for battery and supercapacitor storage system. IEEE Trans Sustain Energy 5(4):1137–1144

22. Kollimalla S, Ukil A, Gooi H, Manandhar U, Tummuru N (2017) Optimization of charge/discharge rates of a battery using a two-stage rate-limit control. IEEE Trans Sustain Energy 8(2):516–529

23. Manandhar U, Tummuru N, Kollimalla S, Ukil A, Beng G, Chaudhari K (2018) Validation of faster joint control strategy for battery- and supercapacitor-based energy storage system. IEEE Trans Ind Electron 65(4):3286–3295

24. Zeraati M, Golshan MH, Guerrero J (2018) Distributed control of battery energy storage systems for voltage regulation in distribution networks with high PV penetration. IEEE Trans Smart Grid 9(4):3582–3593

25. Perdana Y, Muyeen S, Al-Durra A, Simoes M, Morales-Paredes H (2018) Direct connection of supercapacitor-battery hybrid storage system to the grid-tied photovoltaic system. IEEE Trans Sustain Energy 10(3):1370–1379

26. Aktas A, Erhan K, Özdemir S, Özdemir E (2018) Dynamic energy management for photovoltaic power system including hybrid energy storage in smart grid applications. Energy 162:72–82

27. Yi Z, Dong W, Etemadi AH (2018) A unified control and power mangement scheme for PV-battery-based hybrid microgrids for both grid-connected and islanded modes. IEEE Trans Smart Grid 9(6):5975–5985

28. Abdullah M, Yatim A, Tan C, Samosir A (2013) Control of a bidirectional converter to interface ultracapacitor with renewable energy sources. In: 2013 IEEE international conference on industrial technology (ICIT)

29. Zhang J, Lai J-S, Yu W (2008) Bidirectional DC–DC converter modeling and unified controller with digital implementation. In: 2008 Twenty-third annual IEEE applied power electronics conference and exposition

30. Glavin M, Chan P, Armstrong S, Hurley W (2008) A stand-alone photovoltaic supercapacitor battery hybrid energy storage system. In: 2008 13th International power electronics and motion control conference

31. Fu M, Zhang D, Li T (2017) Design and analysis of a conductance compensator for keeping constant bandwidth and output impedance in average current mode control. IEEE Trans Power Electron 32(1):837–848

32. Slah F, Mansour A, Hajer M, Faouzi B (2017) Analysis, modeling and implementation of an interleaved boost DC–DC converter for fuel cell used in electric vehicle. Int J Hydrogen Energy 42(48):28852–28864

33. Jin Y, Xu J, Zhou G, Mi C (2009) Small-signal modeling and analysis of improved digital peak current control of boost converter. In: 2009 IEEE 6th international power electronics and motion control conference